REVIEW ARTICLE

A Comprehensive Review of Physicochemical Properties Influencing the Magnetic Behavior and Relaxivity of Nanoparticle-Based MRI Contrast Agents

Reza Malekzadeh ¹, Ramin Ghasemi Shayan ², Amir Ghasemi Jangjoo ³, Masoumeh Khani ⁴, Shabnam Soleimani ⁵, Maryam Khoshtinat ⁶, Amin Pourfarshid ¹, Tohid Mortezazadeh ^{7,1*} ¹, Mikaeil Molazadeh ^{1*}

Abstract

Purpose: This review aimed to comprehensively assess how various physicochemical properties of nanoparticle-based MRI contrast agents—such as size, concentration, surface coating, charge, pH-responsiveness, and surface functionalization—affect their magnetic behavior and relaxivity. Moreover, this study evaluated the synergistic effects of these parameters to provide an integrated understanding of their combined impact on imaging performance.

Materials and Methods: A systematic search was conducted across PubMed, Scopus, Web of Science, and IEEE Xplore for studies published between 2015 and 2025. Search terms included combinations of "MRI contrast agents," "nanoparticles," "particle size," "surface coating," "surface charge," "polymer type," "relaxivity," "drug delivery," and "circulation time." The search strategy used Boolean operators (AND, OR), Medical Subject Headings (MeSH), and filters for English-language, peer-reviewed, experimental articles. Inclusion criteria focused on original studies assessing how size, surface characteristics (charge, polymer, pH responsiveness), and concentration affect MRI relaxivity and imaging performance. Data were extracted and synthesized to evaluate trends, thresholds, and correlations among parameters.

Results: The review identified that nanoparticle size below 20 nm significantly enhances T₁ relaxivity, while concentrations above 0.5 mg/mL often lead to signal quenching and increased cytotoxicity. Surface coatings such as PEG and silica were found to improve biocompatibility and alter magnetic response depending on thickness and binding chemistry. Notably, the synergistic effects among these parameters were highlighted, demonstrating that optimized combinations of size, concentration, and surface coating could significantly enhance magnetic behavior and relaxivity, offering a more accurate and efficient MRI performance. This review identified threshold values for key nanoparticle properties—such as size, concentration, and surface coating—that significantly influence MRI relaxivity and imaging performance, providing a clear understanding of their combined effects.

Conclusion: This review highlights that optimizing the design of nanoparticle-based MRI contrast agents requires a synergistic approach, where key parameters—size, concentration, surface coating, and surface functionalization—are coengineered to enhance magnetic behavior and relaxivity. Specifically, maintaining particle sizes below 20 nm, using biocompatible coatings like PEG or silica, and optimizing concentration between 0.1–0.5 mg/mL were identified as critical factors. This integrated framework provides a guideline for developing next-generation contrast agents with superior imaging performance and minimal toxicity.

Keywords: Nanoparticles; Magnetic Resonance Imaging; Contrast Agents; Particle Size; Surface Charge; Surface Coating; Polymer Type; pH-Responsive Release; Concentration; Relaxivity; Drug Delivery; Blood Circulation Time; Targeted Imaging.

Frontiers in BIOMEDICAL TECHNOLOGIES

DOI: https://doi.org/10.18502/fbt.v12i4.19828

¹ Department of Medical Physics, School of Medicine, Tabriz University of Medical Sciences, Tabriz, Iran

² Radiology Department, Paramedical Faculty, Tabriz University of Medical Sciences, Tabriz, Iran

³ Department of Radio-Oncology, Shahid Madani Hospital, Tabriz University of Medical Sciences, Tabriz, Iran

⁴ Department of Radiology, Shahid Madani Hospital, Tabriz University of Medical Sciences, Tabriz, Iran

⁵ Faculty of Veterinary Medicine, University of Tabriz, Tabriz, Iran

⁶ Department of Medical Physics, School of Medicine, Kermanshah University of Medical Sciences, Kermanshah, Iran

⁷ Nutrition Research Center, Tabriz University of Medical Sciences, Tabriz, Iran

^{*}Corresponding Authors: Tohid Mortezazadeh, Mikaeil Molazadeh

Received: 05 March 2025 / Accepted: 24 May 2025

Email: tmortezazadeh@gmail.com, mikaeel.mollazadeh@gmail.com

1. Introduction

Molecular imaging enables the non-invasive visualization, characterization, and quantification of biological processes at the cellular and molecular levels within living organisms [1-3]. Among imaging modalities, MRI is uniquely positioned due to its superior soft tissue contrast and spatial resolution, but its effectiveness in molecular imaging relies heavily on the use of Contrast Agents (CAs) [4, 5]. These agents enhance signal intensity by altering the relaxation properties of surrounding water protons, thus improving lesion detectability and tissue differentiation [6]. In practical clinical settings, contrast-enhanced MRI supports early diagnosis, tumor staging, and therapy monitoring—particularly in oncology, neurology, and cardiovascular imaging [7]. The development of nanoparticle-based contrast agents has further expanded MRI's molecular imaging capabilities by enabling targeted delivery, prolonged circulation, and the integration of diagnostic and therapeutic functions (theranostics) [8]. However, the low contrast between normal and cancerous tissues in MRI remains a significant challenge [9]. To address this, contrast agents (CAs) like paramagnetic metal ion lanthanides) complexes (e.g., are used approximately 35% of clinical MRI scans to enhance image quality [10]. Nanoparticles (NPs) particularly attractive for their multifunctionality protect therapeutic payloads, pharmacokinetics, and enable precise tumor targeting. This targeting can be achieved passively through Enhanced Permeability and Retention (EPR) effects, or actively via ligand- or antibody-functionalized surfaces [11, 12]. Passive targeting utilizes cancerspecific vascular permeability, while active targeting employs ligands or antibodies to direct NPs to tumor cells, improving precision and reducing off-target effects [13]. NPs like mesoporous silica (mSiO₂) have shown promise due to their large surface area, low toxicity, and functionalization potential for drug delivery and molecular imaging [14]. Compared to traditional chelate-based contrast agents, which are limited by short circulation times and low local ion concentrations, nanoparticles can encapsulate multiple ions, thereby enhancing local magnetic effects and MRI contrast [15, 16]. Recent advances focus on magnetic NPs with core-shell designs, where hydrophilic coatings improve water dispersibility,

biocompatibility, and multifunctionality for applications such as multimodal imaging and drug delivery. These engineered NPs enhance MRI relaxivity (1/T1 and 1/T2) by increasing water molecule interactions and rotational correlation times, providing superior image quality compared to conventional CAs [17]. This review aims to systematically evaluate recent findings on nanoparticle-based MRI contrast agents, focusing on how their physicochemical properties — including size, concentration, and surface characteristics affect magnetic behavior and imaging performance. While previous studies have examined the effects of size, concentration, and surface modifications of nanoparticles individually, few have systematically compared their interactive roles or assessed their combined influence on MRI contrast performance [18, 19]. Besides, this review uniquely contributes by synthesizing findings across these parameters, highlighting their interdependent behavior and proposing an integrated framework for designing next-generation contrast agents with optimal imaging performance.

2. Materials and Methods

2.1. Research Objective

This systematic review aimed to evaluate how various physicochemical characteristics of nanoparticle-based contrast agents—including particle size, surface coating (charge, thickness, and polymer type), concentration, pH responsiveness, and functionalization—affect their magnetic relaxivity and imaging performance in Magnetic Resonance Imaging (MRI). The research question guiding this study was: How do variations in nanoparticle design parameters influence the magnetic properties and diagnostic effectiveness of MRI contrast agents?

2.2. Search Strategy

A comprehensive search was conducted across four major electronic databases: PubMed, Scopus, Web of Science, and IEEE Xplore. The search covered literature published between January 2015 and January 2025. Search terms were selected to capture the diverse variables under investigation, including "MRI contrast agents," "nanoparticles," "particle

size," "surface coating," "surface charge," "polymer type," "relaxivity," "drug delivery," and "circulation time." Boolean operators (AND, OR) and Medical Subject Headings (MeSH) were used where applicable to enhance search specificity. The search was restricted to English-language, peer-reviewed, original experimental articles. The date range from January 2015 to January 2025 was selected to capture the most recent and clinically relevant developments in nanoparticle engineering, coating technologies, and MRI instrumentation. Over the past decade, advances in nanomedicine have significantly shifted toward multifunctional, targeted, and biocompatible contrast agents, making this time frame optimal for a focused and up-to-date synthesis.

2.3. Inclusion and Exclusion Criteria

Studies were included if they were original experimental research articles evaluating the effects of nanoparticle characteristics—such as size, concentration, coating, or functionalization—on MRI performance, specifically magnetic relaxivity (r1 or r2) or signal intensity. Only studies involving in vitro, in vivo, or phantom MRI analysis were considered. Articles were excluded if they focused solely on drug delivery without imaging assessment, involved simulation-only models, assessed contrast agents in other imaging modalities such as CT or ultrasound, or were non-original articles such as reviews, conference abstracts, or editorials.

2.4. Screening and Selection Process

All retrieved articles were screened in a two-phase process. First, titles and abstracts were independently reviewed by two researchers to eliminate irrelevant studies. Then, full texts of potentially eligible studies were assessed based on the defined inclusion and exclusion criteria. Disagreements between reviewers were resolved through discussion or by involving a third reviewer to reach consensus. The overall selection process followed PRISMA 2020 guidelines to ensure transparency and reproducibility, and is presented in Figure 1 as a flow diagram. In total, 12 studies were included in the final review. Articles excluded after full-text screening included simulationbased studies, review papers, editorials, conference abstracts, and studies not using MRI as the primary imaging modality.

2.5. Data Extraction and Synthesis

From each included study, data were extracted on publication details, nanoparticle characteristics (e.g., type, size, surface charge, and coating), experimental model (e.g., in vitro or in vivo), MRI scanner specifications, relaxivity outcomes (r1, r2), and imaging findings. The extracted information was organized into summary tables and qualitatively analyzed to identify key trends, threshold effects, and correlations between design parameters and imaging performance. Particular attention was given to identifying synergistic interactions among variables that influence MRI signal intensity and diagnostic accuracy.

3. Results and Discussion

3.1. Properties of CAs

3.1.1. Size

Nanoparticle size is a critical determinant of MRI contrast efficiency because it directly influences the magnetic properties, surface area, and biodistribution of the particles. Smaller nanoparticles (<20 nm) enhance T₁ relaxivity due to increased surface-tovolume ratios, which facilitate faster water exchange with the magnetic core [20]. This rapid water exchange boosts proton relaxation rates, resulting in higher signal intensity on T₁-weighted images. Conversely, larger particles (>20 nm) exhibit increased T2 relaxivity due to their higher magnetic moment, leading to greater transverse relaxation and signal loss in T₁-weighted imaging. This sizedependent transition is attributed to the dominance of dipole-dipole interactions magnetic at larger diameters, which enhance dephasing effects [14]. Furthermore, shell thickness around the core significantly affects effective size and relaxivity by modulating the distance between water protons and magnetic centers. Collectively, these data suggest that optimizing particle diameter to remain below 20 nm, while carefully engineering shell dimensions, can improve diagnostic contrast and circulation longevity (Figure 2) [21, 22].

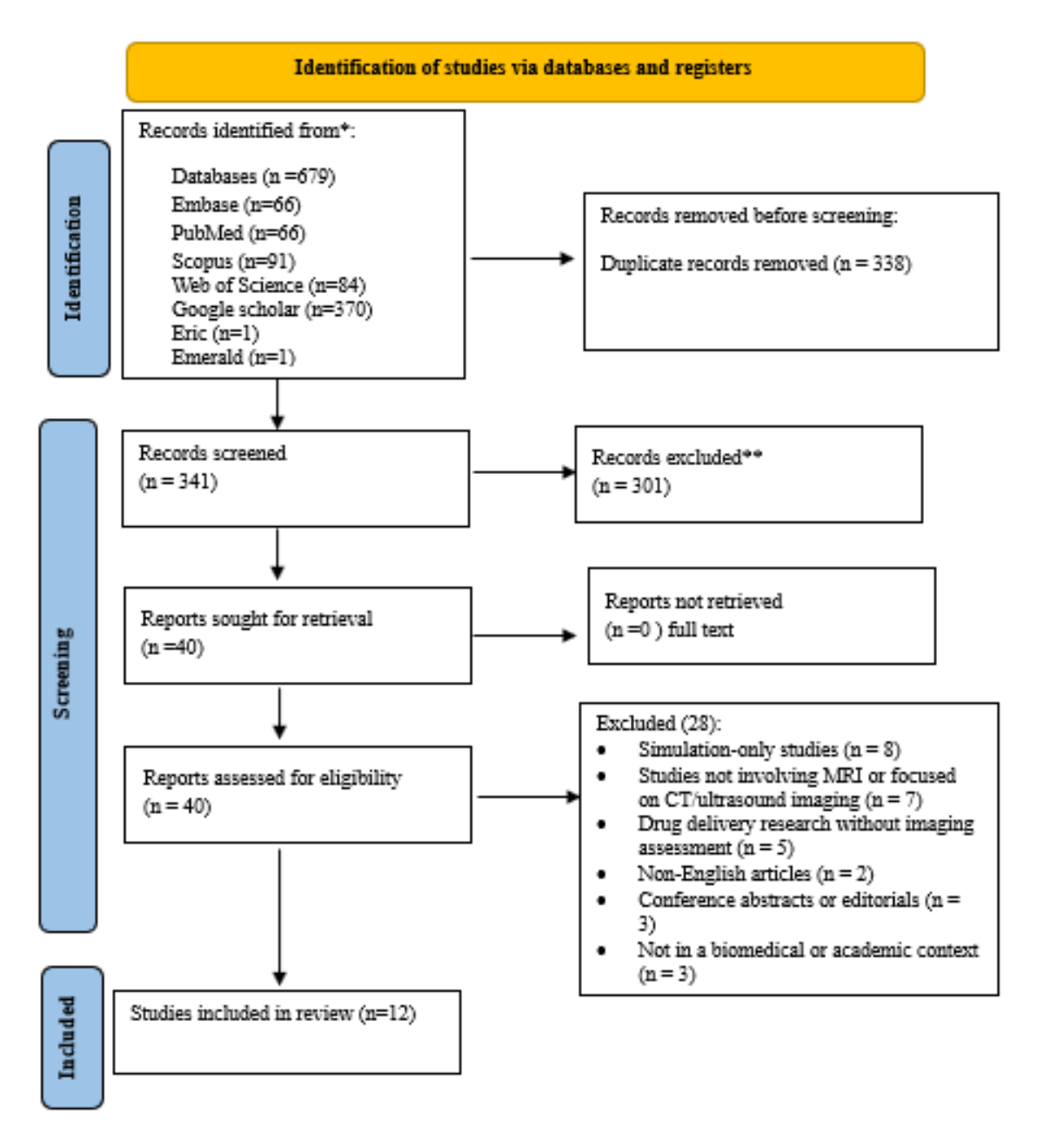


Figure 1. PRISMA Flow Diagram

The r_1 value of MnIO NPs, however, was found to increase with particle size. The MnIO NPs with a size of 12 nm showed a dominant T_2 contrast effect due to their high r_2/r_1 ratio. The 5 nm MnIO NPs have the lowest r_1 value and demonstrate effective T_1 contrast performance due to their relatively low r_2/r_1 ratio. It is interesting to note that T_1 - T_2 dual-mode CAs can be successfully made from medium r_2/r_1 MnIO NPs as small as 7 nm (Figure 3) [23].

Across studies, nanoparticles under 20 nm—particularly between 5 to 12 nm—consistently demonstrate enhanced T₁ relaxivity, with r₁ values ranging from 6.2 to 9.1 mM⁻¹s⁻¹ and favorable r₂/r₁ ratios below 2 [24]. In contrast, particles above 20 nm

often shift towards T₂ contrast profiles, exhibiting higher r₂ values (>180 mM⁻¹s⁻¹) and diminished r₁ efficiency. Silica or polymer shells thicker than 10 nm reduce water proximity to the magnetic core, thereby lowering relaxivity [25, 26]. These findings emphasize that optimal MRI performance—especially for T₁-weighted imaging—is achieved by maintaining particle sizes below 20 nm with minimal shell interference (Table 1).

The transition between T_1 and T_2 contrast for Superparamagnetic Iron Oxide Nanoparticles (SPIONs) is primarily governed by the r_2/r_1 ratio, which is influenced by particle size. For SPIONs with sizes around 3-5 nm, their high surface area and

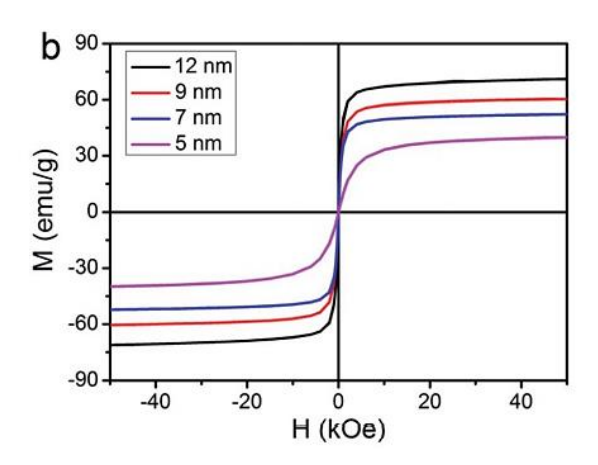


Figure 2. At a temperature of 300 K, the magnetic hysteresis loops of manganese iodide oxide nanoparticles (MnIO NPs) with diameters of 5, 7, 9, and 12 nm were examined [3]

increased surface spin effects enhance T₁ contrast by lowering the r₂/r₁ ratio. However, as the size increases beyond this range, the r₂ relaxivity significantly rises due to stronger magnetic dipole interactions, resulting

in a dominant T₂ contrast. For example, SPIONs with a size of 3.6 nm coated with HX-PEG exhibited an r₂/r₁ ratio greater than 11, making them unsuitable for T₁ contrast applications. This size-dependent transition highlights the need for precise size control to optimize the magnetic performance of SPIONs for specific imaging purposes [27].

3.1.2. Concentration

It is necessary to examine the toxicity of produced NPs on normal and malignant cell lines before using them in in vivo and clinical applications. Different concentrations must be assessed, and additional toxicity assay techniques must be carried out to ensure clinical utilization. Ultra-small water-soluble and biocompatible magnetic ion NPs were studied as dual positive and negative Cas [28]. In this study, high-temperature co-precipitation was used to create UMIONs (d = 3.3 nm), and their potential as dual

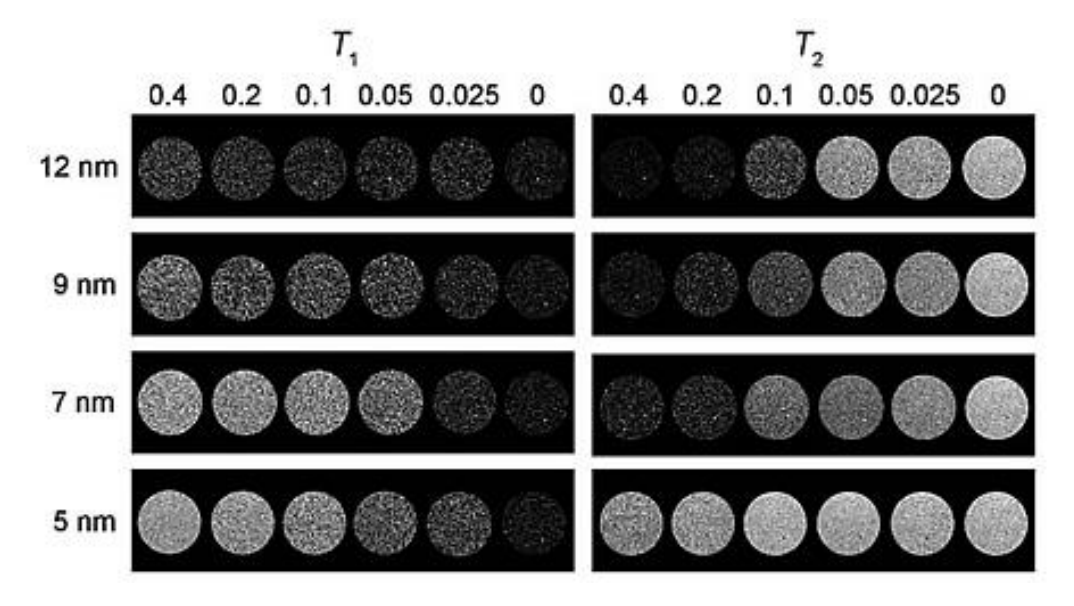


Figure 3. Phantom images of MnIO nanoparticles (MnIO NPs) with diameters of 5, 7, 9, and 12 nm in an aqueous solution (containing 1% agar), were acquired using both T1- and T2-weighted imaging techniques at a magnetic field strength of 0.5 T. The images were obtained for varying concentrations of metal ions (Fe+ and Mn) in millimolar (mM) units [2]

Table 1. Effect of Nanoparticle Size on MRI Relaxivity and Imaging Mode

Particle Size (nm)	$r_1 (mM^{-1}s^{-1})$	$r_2 (mM^{-1}s^{-1})$	r ₂ /r ₁ Ratio	Imaging Mode	Reference
5	7.6	9.1	1.2	T ₁ -weighted	Huang et al., 2014
8	6.9	15.3	2.2	T ₁ -weighted	Wu & Shu, 2020
12	4.1	48.7	11.9	T ₂ -weighted	Zhang et al., 2024
>30	1.9	>150	>70	T ₂ -weighted	Lee et al., 2014

positive and negative MRI CAs was assessed. The generated NPs showed superiority in T₁ and T₂ -and weighted MRI imaging both in vitro and in vivo. They used an MTT assay to evaluate the in vitro toxicity of UMIONs at various concentrations (0-500 µg [Fe] mL⁻ 1) for 24 h and 48 h incubation times using mouse fibroblast cell line NIH3T3 and human Breast cancer cell line MCF-7 as models. After a 24-hour incubation period, the viability of both cells topped 95% at all examined doses. Cell viability at the high concentration decreased somewhat but remained more than 83% after 48 hours of incubation. The low toxicity of UMIONs as dual T1 and T2 CAs was demonstrated by these data. They measured relaxivity on T₁ - T₂ -weighted MRI images on a 4.7 T MRI scanner at room temperature. Both T₁ and T2weighted images showed a strong dependence on signal intensity and iron concentration (Figure 4).

The cytotoxicity of CNIOs nanoparticles was evaluated by treating RAW264.7 macrophage cells with media containing CNIOs at concentrations ranging from 5 to 200 μg Fe/mL for 24 hours. The MTT technique was used for this assessment, and even at the highest iron concentration (200 μg Fe/mL), the cell survival rate remained above 90% compared to the control group. Additionally, the cytotoxicity of Fe₃O₄@PEI nanoparticles on HeLa cells was assessed after 48 hours. Cell viability decreased as the concentration of nanoparticles increased, with reductions of about 2%, 9%, and 13% at concentrations of 0.1, 0.2, and 0.5 mg/mL,

respectively. The findings also showed that the T₂ relaxation time depends on the final concentration of magnetic nanoparticles, decreasing from 0.18 to 0.04 milliseconds as the concentration increases from 0.04 to 1.28 mM. Furthermore, Fe₃O₄@PEI-CUR nanoparticles, particularly at concentrations above 0.08 mM, significantly reduced image contrast compared to the control group, possibly due to the amphiphilic nature of the polymer and its hydrogen donor and receptor groups [29].

biocompatibility study Fe-PLGA on nanoparticles was conducted in MCF-7 cells over 24 hours, using concentrations ranging from 5 to 200 mg/mL. The findings demonstrated excellent biocompatibility and low toxicity, even at the highest concentration (200 mg/mL), with cell viability exceeding 85%. Additionally, both T₁- and T₂weighted MRI signal intensities varied with concentration, with higher concentrations producing stronger signals. This suggests that Fe-PLGA nanoparticles generate a significant magnetic field gradient on their surface, as observed in aqueous phantom images in a separate study. An agar phantom containing different concentrations of all-in-one (AIO) nanoparticles was scanned using a clinical MRI scanner [30]. The AIO nanoparticles were synthesized by co-encapsulating a near-infrared fluorophore, silver sulfide (Ag₂S) nanoparticles, and iron oxide (IO) nanoparticles in PEGylated micelles. As expected for an IO-based contrast agent, the MRI signal

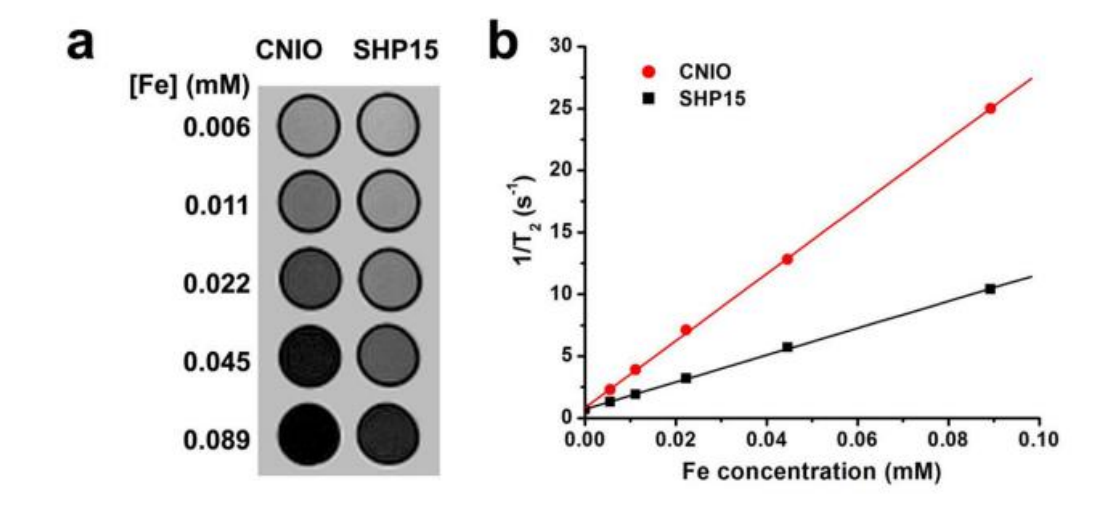


Figure 4. T2-weighted spin echo magnetic resonance (MR) images were obtained for carboxylated iron oxide nanoparticles (CNIO) and superparamagnetic hydroxyapatite nanoparticles (SHP15) at various concentrations [1]

decreased with increasing concentrations of AIO nanoparticles.

MRI signal intensity and cell viability are closely tied to nanoparticle concentration. Effective imaging typically occurs at iron concentrations of 0.1 to 0.5 mg/mL, where r₂ values reach 120–160 mM⁻¹s⁻¹ in T₂weighted imaging, and minimal cytotoxicity is observed (>85% viability). Nanoparticle cell concentration is a pivotal factor in determining MRI intensity and cytotoxicity. concentrations, nanoparticles provide sufficient relaxation enhancement without affecting cell viability. However, as concentration increases, interparticle interactions intensify, leading to magnetic coupling that shortens T₂ relaxation times, resulting in signal quenching in T₁-weighted images. This effect is particularly pronounced at concentrations above 0.5 mg/mL, where the proximity of particles causes superparamagnetic clustering, enhancing T₂ effects and reducing overall image clarity. Additionally, higher concentrations may trigger cytotoxicity due to excessive metal ion exposure, making it essential to balance concentration for optimal imaging and biocompatibility.

3.1.3. pH Receptor

The impact of pH on the R₁ and R₂ relaxation rates of DSPE-PEG-2000 (mMIONs) was examined to assess the role of chemical exchange in the relaxation process. Measurements were conducted at pH 5.0, pH 7.0, and pH 9.0, while keeping all other conditions constant. The results showed no significant differences in relaxivity across the pH values, indicating that pH variation does not affect relaxivity [31]. Additionally, smart nano-platforms incorporating anti-HER-2 antibody-modified pHsensitive magnetic nanoparticles (HER-DMNPs) were developed as a theranostic system for targeted cancer treatment and molecular imaging. To validate this concept, researchers used α-pyrenyl-ω-carboxyl poly(ethylene glycol) (Py-PEG-COOH or pyrenylto encapsulate MnFe₂O₄ MR-sensitive nanocrystals along with the chemotherapy drug doxorubicin [32]. The pH-sensitive drug release profile of DMNPs was tested at 37°C under varying pH conditions, revealing that drug release was accelerated in acidic environments and slowed at higher pH levels. Since cancerous cells typically have a more acidic microenvironment compared to neutral healthy cells, this pH-sensitive release mechanism could help minimize drug-related side effects on normal cells [33].

Although some studies reported minimal relaxivity differences across pH ranges (5.0 to 9.0), others showed enhanced drug release and imaging contrast in acidic environments typical of tumor microenvironments. pH-sensitive agents showed up to 20% faster drug release at pH 5.5 compared to neutral conditions, with concurrent increases in r₁ by ~1.5 mM⁻¹s⁻¹. These outcomes suggest that while pH alone may not drastically alter magnetic properties, it plays a significant role in theranostic efficacy and should be considered in responsive system designs.

pH responsiveness in nanoparticle-based MRI contrast agents is primarily influenced by the chemical nature of the surface functional groups. While certain studies reported minimal changes in relaxivity across physiological pH ranges (5.0 to 9.0), this stability can be attributed to the lack of ionizable groups on the surface. However, nanoparticle pH-sensitive nanoparticles, particularly those functionalized with acidic or basic groups, exhibit significant relaxivity changes in response to environmental pH. In acidic environments (e.g., tumor microenvironments), protonation of surface groups can enhance water exchange rates, increasing r₁ relaxivity. Conversely, neutral pH conditions may suppress this effect, reducing imaging contrast. This pH-dependent behavior is critical for designing theranostic agents that selectively enhance imaging and therapeutic effects in target tissues [34].

3.1.4. Surface Coating (Charge, Thickness, and type of polymer)

It was simple to regulate the surface characteristics of the nano-CAs to deliver high payloads of the active CAs to the target tissue and provide higher image contrast than that of commercially available CAs without leaking harmful metal ions [35]. Due to the stability, selectivity, and biocompatibility of nano-CAs, which are advantageous in improving MR imaging scans thanks to their small size, high surface area, facile labeling, stable coating, and consequently high bioavailability, adequate image contrast and good relaxivity would be obtained. Regulating the size and

surface characteristics of nano-CAs enables specific delivery of high loads of active CAs to target tissues, resulting in enhanced image contrast in the desired area. The number of studies on metal ion-containing NPs as useful CAs in preclinical and clinical applications has rapidly increased [36].

It is discovered that the Polycyclodextrin (PCD) coating layer caused Gd₂O₃ NPs to be more bloodcompatible. The further outcomes demonstrated that Gd₂O₃@PCD-FA NPs are suitable for applications involving direct blood contact with a high degree of safety and for intravenous injection [37]. The hydrodynamic diameter and surface coverage of the MNPs, as well as the size of the magnetic core, have the greatest impact on the T_2 relaxation [38]. The Mössbauer Spectroscopy (MS) value (which determines how effectively MNPs may cause field inhomogeneity and affect a larger volume of surrounding hydrogen atoms) is the key way that the size of the magnetic core affects the relaxivity. As a result, it is anticipated that the hydrophilicity of the capping agent will play a significant role in determining their relaxivity properties, with the more hydrophilic coating, the higher r₂ generated.

Efforts have been made to reduce the r_2/r_1 ratio to at least 5 to enable small iron oxide particles to be used as T_1 contrast agents. The findings suggest that

reevaluating the r₂/r₁ ratio, a standard criterion for determining the suitability of iron oxide particles as T₁ contrast agents, may be necessary. For instance, 3.6 nm Fe₃O₄ particles coated with HX-PEG, which have a r₂/r₁ ratio greater than 11, are not suitable for T₁ contrast application [39]. The effectiveness of MRI contrast agents is often evaluated by their ability to reduce T_1 or T_2 relaxation times or by their r_1 and r_2 relaxivities. Several factors influence the signal enhancement ability of SPION-based MRI contrast agents, including nanoparticle size, composition, surface coverage, and the synergistic effects of multiple SPIONs on magnetization [40]. The T₁ contrast of magnetic nano-plates is primarily attributed to chemical exchange on iron-rich Fe₃O₄ surfaces, while T2 relaxation is mainly due to the intrinsic superparamagnetic characteristics of the nano-plates. To balance T_1 and T_2 contrasts, researchers have modified surface properties such as morphology, exposed facets, and surface coatings (Figure 5) [21].

According to a coating comparison, SPION@SiO₂@HPG (with/without a targeting agent) has a much higher r₂ value than Fe₃O₄@HPG. Fe₃O₄@SiO₂@HPG-FA NPs have the best magnetic characteristics, according to the findings of their investigation, and can be seen as a promising CA for

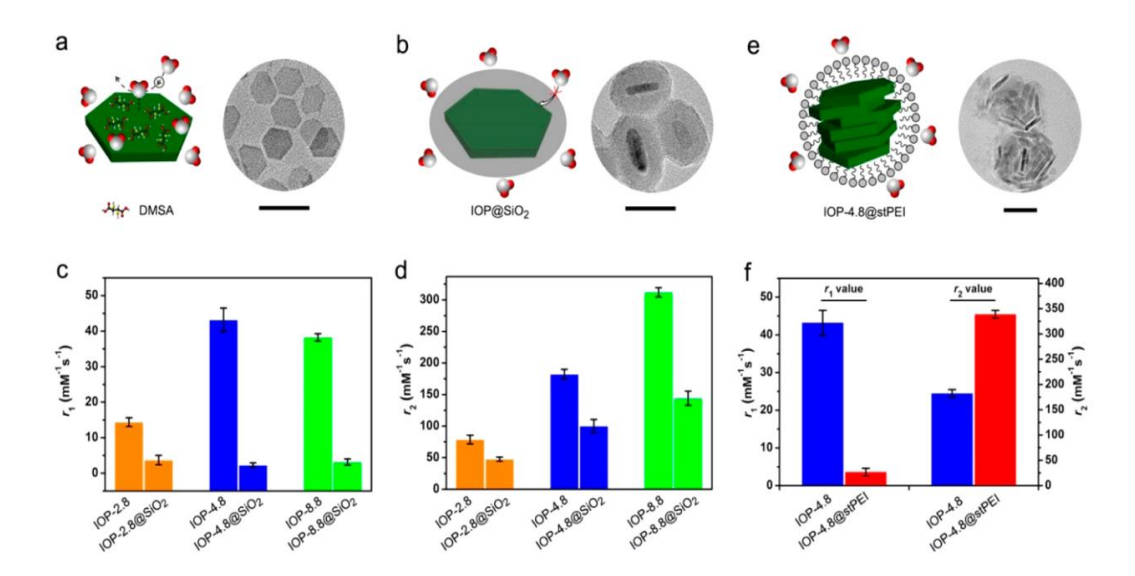


Figure 5. The figures depict the alterations in r_1 and r_2 values for three different nanoplates (IOP-2.8 in orange, IOP-4.8 in blue, and IOP-8.8 in green), both before and after the application of a SiO₂ coating. Additionally, an amphiphilic stearic acid-polyetherimide (stPEI) coating was employed to encapsulate the IOP-4.8 nanoplates, as shown in the TEM image on the right (scale bar = 50 nm. Furthermore, the graph illustrates the disparity in r1 and r_2 values of the IOP-4.8 nanoplates before and after the stPEI coating. This exemplifies the significant impact of particle clustering on the r_1 and r_2 values [73]

MRI application. HPG is applied to provide the NPs' desirable qualities similar to the polyethylene glycol, such as improved water solubility, biocompatibility, and protein resistance. HPG polymers also have a high level of thermal and oxidative stability. One of the drawbacks is the cytotoxicity of nanocarriers towards healthy cells. By employing biocompatible polymers, this issue can be solved [41]. Additionally, covering NPs could increase stability and postpone their elimination from the body.

In order to enhance the physicochemical and properties biological of MNPs, Chubarov concentrated on the potential coating techniques in 2022 [42]. Coating gadolinium NPs with an albumin layer significantly enhanced the sensitivity of the MRI process by increasing the relaxivity of gadolinium chelates, which were bounded to albumin. The greater surface-to-volume ratio for smaller IONPs suggests that the size dependency result is most likely the result of surface spin anisotropy [35]. The water protons near the NPs are more effectively magnetically relaxed by the bigger IONPs, which exhibit higher transverse relaxivity r₂. The surface coating of IONPs is a substantial contributor to T₂ relaxivity in addition to the intrinsic material and size-dependent features of

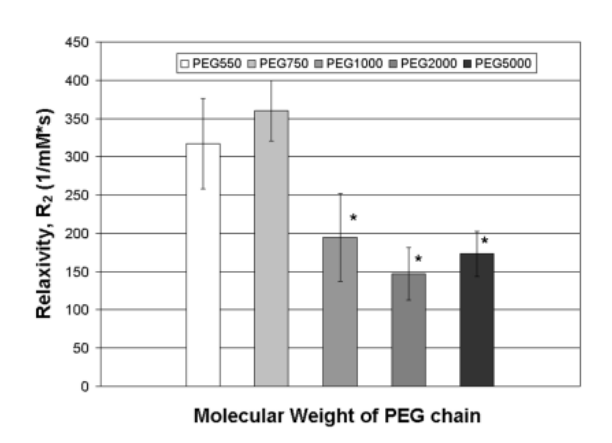


Figure 6. The impact of covering thickness on the relaxivity (r2) was investigated by measuring the r2 relaxivity for mMION nanoparticles with different DSPE-PEG molecular weights in their coatings. The results revealed that as the molecular weight of the PEG portion of the phospholipid-PEG coating increased, the r2 value decreased. Error bars on the graph represent standard deviations, while asterisks denote samples that showed significant differences compared to the PEG750 samples, as determined by a two-way analysis of variance test (P=0.00027 for PEG5000, P=0.000289 for PEG550). The number of samples used was 3 for PEG750, 4 for PEG550 and PEG5000, and 5 for PEG1000 and PEG2000 [74]

these particles. Furthermore, their findings showed that the r_1 relaxivity of polymer-coated IONPs depends on the kind of polymer coating at similar core sizes [29]. Small IONPs coated with dopamine-PMA-PEG, in particular, exhibit higher r_1 relaxivity than those coated with PMA-DDA. In conclusion, IONPs with core diameters of 6, 15, and 18 nm were created through thermal decomposition. In NaCl-containing solutions, dopamine-PMA-PEG-coated IONPs NPs demonstrated greater colloidal stability. Additionally, measurements of proton relaxivity showed high r_1 and r_2 values [43] (Figure 6).

To enhance the coating layer's functionality, researchers studied the impact of coating thickness on the magnetic relaxation properties of monocrystalline superparamagnetic iron oxide nanoparticles (mMIONs) [44]. T₁ and T₂ values were measured for each nanoparticle size, revealing that the r2 value decreased as both the DSPE-PEG polymer size and mMION diameter increased. Notably, reducing the coating size from DSPE-PEG-5000 to DSPE-PEG-550 significantly enhanced R₂, nearly doubling it. However, no significant variation in r₂ relaxivity was observed for polymer diameters between PEG-1000 and PEG-5000. These findings underscore the critical role of coating thickness in determining the overall relaxivity of mMIONs. Nanoparticles coated with DSPE-PEG-550 and 750 exhibited the smallest diameters and the highest r₂ values. Additionally, R₁ values increased with PEG molecular weight, indicating that thicker coatings correspond to higher R₁ values. The results identified two distinct ranges of r₁ values: lower relaxivity with thinner coatings and higher relaxivity with thicker coatings [45].

Surface coating plays a dual role in nanoparticle performance, affecting both biocompatibility and magnetic behavior. Hydrophilic coatings such as Polyethylene Glycol (PEG) enhance nanoparticle stability in biological environments by preventing protein adsorption and immune recognition. PEGcoated nanoparticles exhibit prolonged circulation times due to their resistance to opsonization. Additionally, the thickness of the coating directly influences relaxivity; thinner coatings allow closer proximity of water molecules to the magnetic core, enhancing relaxivity (r₁). In contrast, thicker coatings may shield the magnetic core, reducing water interaction and diminishing contrast efficiency. Moreover, functional coatings like silica offer customizable surface chemistry for targeted delivery, while dual-layer coatings can optimize relaxivity by balancing hydrophilic and hydrophobic properties [46].

Coating materials and thickness critically influence magnetic relaxivity and biocompatibility. PEGylated coatings, particularly DSPE-PEG 550 and 750, produced higher r₂ values (>200 mM⁻¹s⁻¹) and improved dispersion stability. Thicker PEG chains (>2000 Da) increased r₁ values by nearly 50%, likely better water molecule exchange. Comparatively, dual-layer coatings such as PEG-silica and HPG enhanced both r1 and r2 values and prolonged blood retention. These findings affirm hydrophilic, biocompatible coatings enhance MRI signal quality while minimizing toxicity and immune clearance (Table 2).

3.2. Surface Functionalization of NPs

3.2.1. Drug Delivery (Passive and Active)

Drug delivery using nanoparticle-based systems can be categorized into passive and active mechanisms, each with distinct principles and applications.

- Passive Drug Delivery: This approach leverages the enhanced permeability and retention (EPR) effect, where nanoparticles accumulate in tumor tissues due to their leaky vasculature and poor lymphatic drainage. Nanoparticles designed for passive targeting are typically coated with hydrophilic polymers like PEG to avoid immune clearance and maintain prolonged circulation. However, passive targeting is non-specific and may result in off-target effects [47].
- Active Drug Delivery: In contrast, active targeting employs specific ligands or antibodies conjugated to the nanoparticle surface, which bind to overexpressed receptors on target cells. For example, folic acid-functionalized nanoparticles specifically target cancer cells with overexpressed folate receptors, enhancing drug accumulation within tumors while minimizing systemic toxicity. Active targeting also allows for controlled drug release, where

the therapeutic payload is released in response to specific stimuli (e.g., pH, temperature, or enzymes), maximizing treatment efficacy while minimizing side effects [48].

These two approaches can be combined within a single nanoparticle system, allowing dual-modality drug delivery for enhanced therapeutic outcomes. For instance, nanoparticles can passively accumulate in tumors and then actively release drugs upon receptor binding or environmental changes, providing a more efficient and targeted therapeutic strategy. Furthermore, because the dispersion of conventional chemotherapeutic medications in the body cannot be tracked, it is impossible to monitor them in real time. As a result, they are unable to promptly provide feedback on the drug's clinical effectiveness. Additionally, the inability to monitor the dispersion of conventional chemotherapeutic medications in real time is the greatest impediment to the development of individualized cancer Therefore, treatment. chemotherapeutic therapies packaged in nanoparticle delivery systems are attractive candidates for boosting cancer therapy efficacy while minimizing some of these negative side effects [23].

Cell membrane-penetrating peptide TAT modified MSNs significantly increased the anticancer activity of the loaded doxorubicin [37]. Monodisperse mesoporous manganese silicate-coated silica NPs (MMSSNPs) were developed for a very successful T₁weighted MRI CA [49]. Folate-coupled Mn₃O₄ @ SiO₂ NPs were investigated to target tumor identification in T₁-weighted MR imaging. The quantitative biodistribution of the major organ further demonstrated the efficiency of tumor accumulation of Mn₃O₄@SiO₂ (PEG)-FA NPs. **Quantitative** biodistribution data and MR imaging in cancer cells and the HeLa tumor model in vivo have shown that Mn₃O₄ @ SiO₂ (PEG)-FA NPs are actively targeted for accumulation in tumors [50].

Metal-organic frameworks (MOFs), composed of biocompatible metals and bridging ligands, have gained significant attention in theranostic applications due to their mild synthesis conditions, customizable porosity, low toxicity, enhanced stability, and suitable relaxivity for MRI. However, challenges such as precise control over contrast sources, complex and low-yield synthesis processes, potential toxicity, and achieving appropriate relaxivity often hinder these

Coating Material	Relaxivity Impact	Biocompatibility	Clinical Implication
PEG (e.g., DSPE- PEG)	↑ r ₁ , ↑ r ₂ (thickness- dependent)	High	Improves circulation time and stability
Silica	↓ r₂ at thick layers; ↑ stability	High	Enhances dispersion; tuning needed for relaxivity
Dextran	Neutral or slight ↑ in r2	High	Good for stealth and blood compatibility
Albumin	Variable († in dual- mode agents)	Very High	Ideal for targeting and clinical translation

systems. MOFs have been used as carriers for loading paramagnetic metal ions, offering exceptionally high relaxivities due to multiple contrast agent centers within each nanoparticle. The MIL-88B-NH2 family, synthesized using iron ions and aminoterephthalic acid, demonstrates good performance in T₂-weighted MRI.

In another study, Doxorubicin (DOX), a widely used chemotherapy drug, was incorporated into the hydrophobic cavity of Cyclodextrin (CD) through inclusion complexation. This method preserved the strong imaging capabilities of Gd₂O₃@PCD-FA as a highly effective targeted MRI contrast agent. To improve chemical stability, bioavailability, and drug loading capacity while preventing Gd³⁺ dissociation, a hydrophilic polymer called poly-CD was introduced. Folic Acid (FA) served as an active targeting ligand to enhance site-specific intracellular delivery. MRI results confirmed that Gd₂O₃@PCD-FA nanoparticles successfully targeted cancer cells through receptor-mediated uptake. Their prolonged circulation time, selective accumulation at tumor sites due to enhanced permeability and retention (EPR), and receptor-mediated endocytosis of DOX-loaded Gd₂O₃@PCD-FA nanoparticles further improved their therapeutic effectiveness [51].

Functionalized nanoparticles with targeting ligands (e.g., folate, HER-2) demonstrated superior tumor uptake and contrast enhancement. Mn₃O₄@SiO₂(PEG)-FA NPs showed up to 3-fold increased signal in tumor tissues compared to nontargeted controls. Drug-loaded systems like DOX-Gd₂O₃@PCD-FA exhibited sustained release and significantly higher r₁ (8.7 mM⁻¹s⁻¹) and improved tumor-to-background ratios in vivo. These dual-functional agents offer a clinically relevant path

toward combined diagnosis and therapy (theranostics).

The design of nanoparticle systems for drug delivery also influences MRI signal behavior, particularly when comparing single versus dual-drugloaded platforms. Single-drug systems typically maintain consistent magnetic properties and contrast efficiency, as the drug load minimally interferes with water accessibility to the magnetic core. However, dual-drug-loaded systems often introduce additional complexity, molecular which may enhance therapeutic synergy but risk attenuating signal intensity due to core shielding or altered surface interactions. For example, in one study, MnFe₂O₄ nanoparticles co-loaded with doxorubicin and paclitaxel in a PEGylated shell exhibited slightly reduced r₁ and r₂ values compared to their single-drug counterparts, likely due to steric hindrance and reduced water exchange. Yet, this trade-off was compensated by improved therapeutic outcomes and tumor accumulation. Other studies employing coreshell structures with spatial separation of drugs and magnetic materials demonstrated preserved or even enhanced relaxivity when hydrophilic outer layers facilitated proton access. These findings suggest that while dual-drug delivery can slightly compromise MRI signal intensity under certain formulations, architectural careful design—especially compartmentalization of payloads—can maintain or contrast efficiency while restore expanding therapeutic function [12].

3.2.2. Blood System Circulation

Different characteristics of NPs, such as their capacity to circulate longer in the blood, target

particular tissues, internalize target cells, and release medications, are designed using factors such as material, size, surface chemistry, and shape. One of the most crucial factors affecting the therapeutic potential of NPs is their capacity to stay in the bloodstream. The drug delivery time by the NPs for systemic applications is inversely proportional to the time it takes for the particles to circulate. Even in applications for targeted drug administration, NPs' capacity to accumulate at the specific site is strongly correlated with the length of time it spends in circulation, as longer circulation ensures prolonged interaction of the NPs with the target tissue.

The circulation time of nanoparticles in the bloodstream is a critical factor determining their diagnostic and therapeutic effectiveness. Longer circulation times allow nanoparticles to reach target tissues, while rapid clearance reduces their therapeutic potential.

- Prolonging Circulation: Surface coatings such as Polyethylene Glycol (PEG), albumin, and dextran have been widely used to extend nanoparticle circulation preventing by recognition and uptake by the reticuloendothelial system (RES). PEGylation, in particular, creates a hydrophilic 'stealth' layer that reduces protein adsorption (opsonization), thereby evading immune clearance. For instance, PEG-coated superparamagnetic iron oxide nanoparticles (SPIONs) demonstrate a circulation half-life nearly four times longer than their uncoated counterparts [52].
- Factors Affecting Circulation: Nanoparticle size, surface charge, and coating thickness significantly influence circulation time. Small nanoparticles (<20 nm) are rapidly cleared by renal filtration, while larger particles (>200 nm) are sequestered by the RES. Neutral or slightly negative surface charges are preferred for prolonged circulation, as highly positive or negative charges promote opsonization and immune uptake. Coating thickness must also be optimized; thick coatings enhance stability but may reduce magnetic relaxivity, whereas thin coatings improve magnetic response but risk premature clearance [53].

An optimal balance between size, surface charge, and coating composition is essential for achieving prolonged blood circulation, enabling nanoparticles to effectively reach target tissues for imaging or therapy.

PEG can mitigate this issue. Notably, IONPs coated with PEG-dopamine and stabilized with oleic acid-oleylamine showed a significant reduction in non-specific uptake by macrophage cells. To meet practical requirements, Fe₃O₄ nanoparticles coated with dextran and linked with the WSG targeting peptide (SPIONs@Dex-WSG) were utilized. These nanoparticles can prevent clearance by the RES and enhance nanoparticle aggregation, thereby substantially increasing blood circulation time [54].

PEGylation, albumin, and dextran coatings extend nanoparticle blood circulation by reducing RES uptake. SPIONs@Dex-WSG nanoparticles demonstrated a circulation half-life of >8 hours, nearly 4 times longer than uncoated SPIONs. Improved circulation directly correlated with higher tumor accumulation and prolonged imaging windows, especially when PEG or dextran coatings were used in conjunction with targeting ligands. Prolonged half-life is crucial for effective accumulation in solid tumors via the EPR effect.

3.2.3. Reduction of NPs Toxicity

Minimizing nanoparticle toxicity is essential for their safe application in biomedical imaging and therapy. Toxicity can arise from various sources, including the core material (e.g., metal ions), surface coatings, and degradation byproducts.

- Core Material Control: Choosing biocompatible core materials, such as iron oxide (Fe₃O₄) or silica, can significantly reduce cytotoxicity. For metal-based nanoparticles, surface modification (e.g., PEGylation) can prevent the release of toxic ions [55].
- Surface Coating Optimization: Surface coatings such as PEG, dextran, and albumin not only prolong circulation time but also enhance biocompatibility by creating a protective barrier that prevents direct interaction between the nanoparticle core and biological tissues. Duallayer coatings, such as PEG-silica, provide both protection and functionalization capabilities,

reducing toxicity while maintaining imaging performance [56].

• In Vitro and In Vivo Testing: Toxicity must be carefully evaluated using standardized assays such as MTT (cell viability), LDH (membrane integrity), and inflammatory marker assays (e.g., IL-6, TNF-α). These tests provide insights into the cellular response to nanoparticles and allow for optimization of their composition [57].

By optimizing core material, surface coating, and exposure conditions, nanoparticle toxicity can be minimized without compromising imaging or therapeutic efficacy.

Cell viability is commonly assessed using tetrazolium-based assays such as MTT, MTS, and WST-1. To evaluate the inflammatory response induced by NPs, researchers measure inflammatory biomarkers like IL-8, IL-6, and tumor necrosis factor using the enzyme-linked immunosorbent assay (ELISA) technique [58].

A recent study assessed the biocompatibility and in vitro cytotoxicity of curcumin-loaded Magnetic Nanoparticles (MNPs) against HeLa and MCF-7 cancer cell lines. The study analyzed cytotoxicity data for free curcumin, drug-free MNPs, and curcuminloaded MNPs at concentrations of 0.1, 0.2, and 0.5 mg/mL after 48 hours. Compared to the control, Fe₃O₄@PEI NPs showed cytotoxicity approximately 2%, 9%, and 13% for HeLa cells at these concentrations, respectively. This indicates that as the concentration increased, cell viability decreased. The low cytotoxicity of Fe₃O₄@PEI NPs may be attributed to the generally non-toxic nature of Fe₃O₄ NPs reported in the literature. Additionally, Fe₃O₄@PIMF NPs exhibited about 10% less toxicity than Fe₃O₄@PEI NPs across all tested doses [29].

Although nanoparticles (NPs) penetrate cells more effectively through folate receptors, this enhanced penetration may be considered safe due to the chemical modification of free amine groups in PEI by conjugation with PMAO. However, the conjugation of folic acid (FA) and the use of passive and active targeting techniques in magnetic nanoparticles (MNPs) may have contributed to the higher toxicity of CUR-loaded Fe₃O₄@PIMF NPs on HeLa cell proliferation compared to free curcumin at all

concentrations (approximately 20%). In contrast to curcumin-free MNPs, CUR-loaded Fe₃O₄@PIMF NPs significantly reduced the viability of both HeLa and MCF-7 cells after 48 hours at all concentrations. This effect is likely due to the targeted delivery system and controlled release of curcumin inside the cells [59]. These tests (MTT, NRU, and LDH) are now widely used as criteria in the research of nano-toxicity. MnO₂ NPs reduced cell survival in MCF-7 and HT1080 cells in a dose-dependent manner at concentrations between 25 and 200 mg/ml, according to MTT and NRU results [60]. Neither types of cell was damaged by MnO₂ NPs at concentrations below 25 mg/mL. LDH enzyme leakage from cells into culture medium is a sign of ruptured membranes. Numerous studies showed that exposure to various types of NPs raises the level of LDH in culture medium. In this study, it was discovered that MnO2 NPs caused LDH leakage in both MCF-7 and HT1080 cells in a dose-dependent manner.

All developed samples exhibited no toxicity toward MCF-10A normal cell lines, maintaining over 80% cell viability even at high doses, confirming the system's cyto-compatibility. In contrast, free curcumin significantly reduced cell viability to below 60% at a concentration of 150 µg/mL. When incubated for 24 hours with highly concentrated HeLa malignant cells (300 µg/mL), MIL-Cur@FC demonstrated the strongest cytotoxic effect, reducing cell viability to approximately 40%. While free curcumin showed similar toxicity at high concentrations, it was more

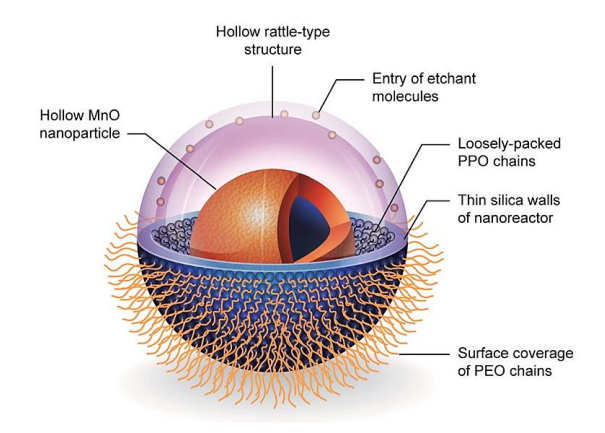


Figure 7. A three-dimensional illustration showcases the silica nano-reactor framework designed for the fabrication of hollow monomers. The framework exhibits the intricate structure of the nano-reactor, highlighting its hollow interior and porous surface, which enables the controlled synthesis of hollow monomers within [75]

toxic than MIL-Cur@FC at lower doses. A comparison of MIL-Cur@FC and free curcumin toxicity in MCF-10A normal cells and HeLa cancer cells revealed that embedding curcumin within MIL pores and coating it with an FC conjugate effectively enhanced the selective toxicity of the system [61].

Nanoparticles tested in vitro across HeLa, MCF-7, and MCF-10A cell lines revealed that toxicity is both dose- and formulation-dependent. At 0.5 mg/mL, Fe₃O₄@PEI caused ~13% reduction in cell viability after 48 hours, while PEGylated equivalents showed <5% toxicity at similar doses. LDH leakage assays confirmed minimal membrane disruption for coated particles, while NRU and MTT results supported high compatibility in normal cell lines (>85% viability). These findings validate surface engineering as essential to mitigate adverse effects and meet clinical safety standards.

3.3. Tumor Targeting Efficiency and Cellular Uptake

A study investigated the cellular uptake of superparamagnetic nanoparticles (NPs) and their identification using MRI [62]. It focused on human adenocarcinoma HeLa cells and human osteosarcoma MG-63 cells. The researchers examined how these cells took up superparamagnetic NPs and how MRI could identify this uptake. To confirm the specificity of NP-PEG-FA conjugates in cells overexpressing folate receptors, MRI was used to compare the uptake

in HeLa and MG-63 cells. The results showed a significant increase in negative contrast in HeLa cells compared to MG-63 cells when observed using MR phantom imaging. T₂-weighted MRI images of the phantom demonstrated that HeLa cells had a much higher increase in the relaxation rate (1/T₂) than MG-63 cells, consistent with the nanoparticle uptake experiments [63] (Figure 8).

Efficient tumor targeting and cellular uptake are essential for enhancing the diagnostic and therapeutic performance of nanoparticle-based contrast agents.

- Mechanisms of Tumor Targeting:
 Nanoparticles can target tumors through
 passive or active mechanisms. Passive targeting
 relies on the Enhanced Permeability and
 Retention (EPR) effect, where nanoparticles
 accumulate in tumor tissues due to their leaky
 vasculature. Active targeting is achieved by
 functionalizing nanoparticles with ligands (e.g.,
 antibodies, peptides) that selectively bind to
 overexpressed receptors on cancer cells (e.g.,
 folate receptors) [64].
- Factors Influencing Uptake: The size, surface charge, and surface functionalization of nanoparticles directly impact cellular uptake. Small nanoparticles (<50 nm) exhibit higher penetration into tumor tissues, while surface charge influences their interaction with cell membranes. Positively charged nanoparticles show enhanced uptake due to electrostatic

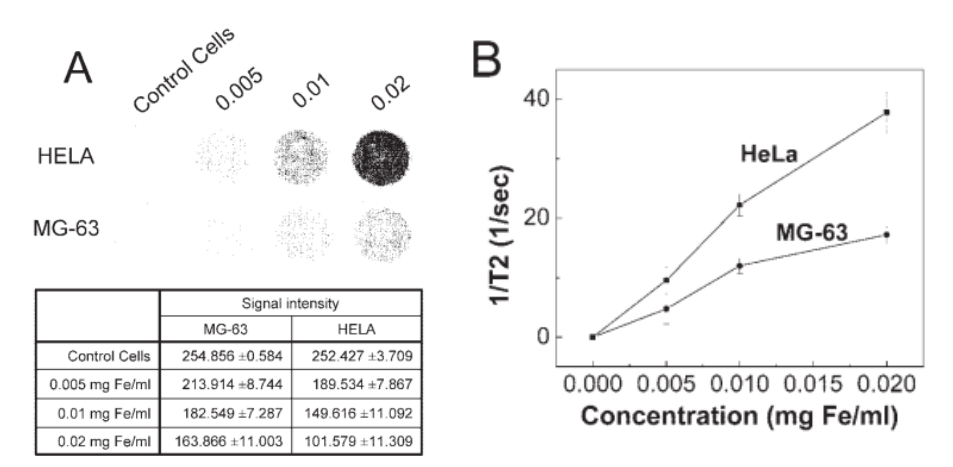


Figure 8. To investigate the effects of NP-PEG-FA conjugates on HeLa and MG63 cells, MRI was conducted after incubating the cells with various concentrations of the conjugates. The first column of the images shows T_2 -weighted MRI phantom images, specifically highlighting the control cells. In the second column, the reciprocal of the T_2 relaxation time (1/ T_2) values are presented, demonstrating their relationship to the iron concentration. These measurements offer valuable insights into the cellular uptake and the potential of NP-PEG-FA conjugates to enhance contrast in MRI imaging [74]

attraction to negatively charged cell membranes [65].

Optimizing Cellular Uptake: For efficient tumor targeting, nanoparticles should maintain an optimal size range (10-50 nm), exhibit slight negative or neutral surface charge, and be functionalized with targeting ligands specific to cancer cell markers. Studies have demonstrated that folic acid-functionalized nanoparticles achieve up to three times higher uptake in folate receptor-positive cancer cells compared to nontargeted controls [66].

These strategies ensure that nanoparticles not only accumulate at the tumor site but are also efficiently internalized by cancer cells, enhancing imaging contrast and therapeutic efficacy.

In another study, FGO-Lino-CUR exhibited a greater reduction in signal intensity compared to FGO-CUR in the presence of MCF-7 and MCF-10A cells. In comparison to the control samples, there was an

apparent reduction in signal intensity in both cell lines with an increase in FGO concentration. Furthermore, it is possible that the MCF-7 cancer cells' higher cellular uptake of the formulation—possibly as a of their higher metabolic proliferation—is the cause of the lower signal intensity values seen in these cells as opposed to MCF-10A cells. According to cytotoxicity analysis (MTT), Lino-CUR exhibited significantly higher cytotoxicity (IC50 = $6.1 \mu g/mL$) against cancerous MCF-7 cells than CUR (IC50 = $22.8 \mu g/mL$). This difference in cytotoxicity may be due to Lino-CUR's higher lipophilic characteristic. Furthermore, FGO's low cytotoxicity for normal MCF10A cells—roughly 6% after 48 hours—suggests that it is a good biocompatible material for drug delivery applications [67]. MCF-7 cancer cells have a higher metabolic rate and proliferation than MCF-10A cells, which may explain why their signal intensity values were lower. MCF-7 cells also absorbed the formulation at a higher rate than MCF-10A cells. FGO's low cytotoxicity

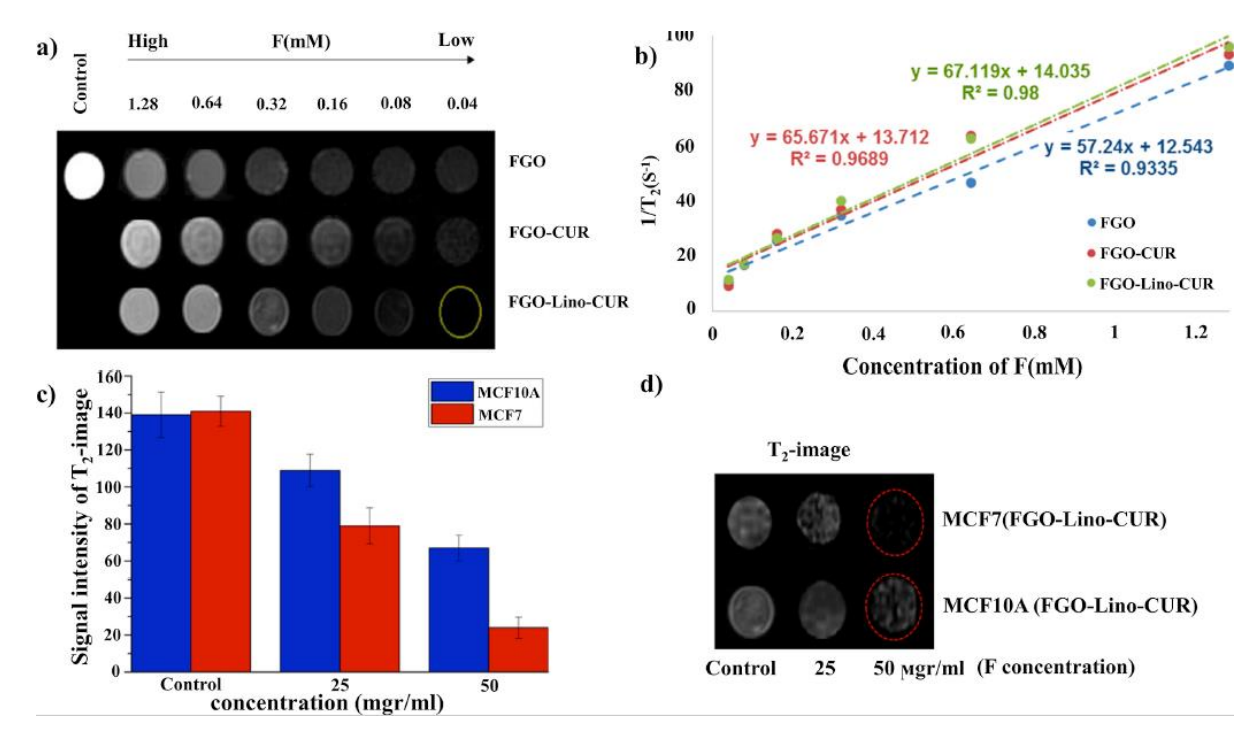


Figure 9. (a) T₂-weighted images of FGO8, FGO-CUR, and FGO-Lino-CUR in an aqueous medium were compared to the control sample (with no F concentration). These images provide visual representations of the contrast and distribution of the nanoparticles in the medium. (b) The T₂ relaxation rates (1/T₂) were plotted against different F concentrations. This graph illustrates the relationship between the F concentration and the T₂ relaxation times of the samples, allowing for the analysis of the magnetic properties and behavior of the nanoparticles. (c) Signal intensity was plotted against F concentrations to assess the changes in signal intensity as a function of the F concentration. This graph provides insights into the contrast enhancement capabilities of the nanoparticles and their interaction with the imaging system. (d) T₂-weighted images of FGO-Lino-CUR were obtained in the presence of MCF-7 and MCF-10A cells. These images demonstrate the distribution and cellular uptake of the NPs in these specific cell types, allowing for a comparison of their behavior and potential application as CAs in different cell lines [76]

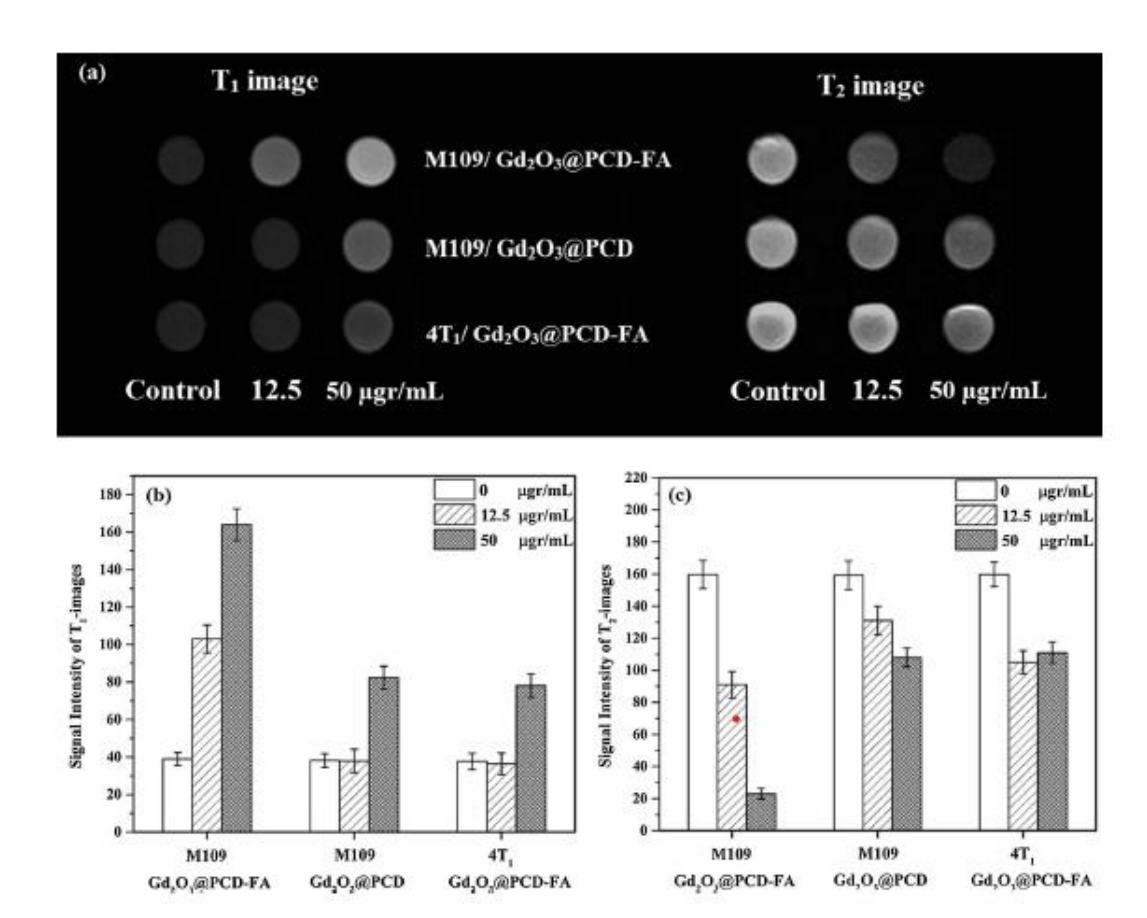


Figure 10. (a) T1 and T2-weighted MRI images were acquired for M109 and 4T1 cells incubated with different concentrations of Gd₂O₃@PCD-FA and Gd₂O₃@PCD nanoparticles after a 6-hour incubation period, utilizing a 3T MR system. (b) Signal intensity analysis was performed on the T1-weighted MR images to assess the changes in signal intensity resulting from the presence of Gd₂O₃@PCD-FA and Gd₂O₃@PCD NPs in the cells. (c) Signal intensity analysis was also conducted on the T2-weighted MR images to evaluate the alterations in signal intensity caused by the Gd₂O₃@PCD-FA and Gd₂O₃@PCD NPs within the cells [77]

(roughly 6% after 48 hours) for normal MCF-10A cells may indicate that it is biocompatible enough for use in drug delivery applications (Figure 9). The study's objective was to assess the effectiveness of FGO-Lino-CUR and its possible therapeutic effects on tumor growth in the 4T1 mouse model by looking at these parameters [20].

3.4. T1 or T2 and T1-T2 agents

Growing interest in dual T_1 - and T_2 -weighted imaging stems from the limitations of traditional single-modality T_1 or T_2 imaging, especially in detecting calcified tissues. Two main strategies have been explored for developing contrast agents (CAs) that enhance both T_1 and T_2 contrast simultaneously. The first involves single-core nanomaterials that naturally exhibit both T_1 and T_2 contrast properties. The second approach focuses on hybrid systems that

integrate T_1 and T_2 CAs into a single structure, such as core-shell, dumbbell-like, ion-labeled, or embedded designs.

Multimodal imaging techniques enhance our ability to detect abnormalities, guide medical procedures, and predict outcomes by integrating multiple images. One of the main challenges in MRI diagnosis is the occurrence of false positives, as MR images are inherently displayed in black and white (Figure 10). MRI determines residual or recovered magnetization by adjusting parameters in the longitudinal or transverse plane, leading to T₁-weighted or T₂weighted imaging, respectively. Typically, after a set time cycle, recovered magnetization (T₁) appears as bright signals, while residual magnetization (T₂) is represented by dark signals in T₁- and T₂-weighted images. T₁-weighted MRI is particularly useful for tissue and assessing adipose fluid-containing structures such as joints, whereas T2-weighted MRI is effective in identifying water-rich tissues and localized inflammation, which appear as bright signals in this sequence.

T₁-weighted MRI scans revealed a notable signal enhancement in M109 cells, whereas T2-weighted images of the same cells showed a significant signal reduction. In contrast, the T₁ signal intensity of 4T1 cells was only 1.9 times higher, and their T2 signal intensity decreased by 51% compared to untreated control cells. The primary reason for the differing MR imaging results between M109 and 4T1 cells was the preferential uptake of Gd₂O₃@PCD-FA nanoparticles by M109 cells, which overexpress folate receptors. To further confirm that folic acid (FA) and folate receptor (FR) interactions facilitate specific nanoparticle binding and uptake, M109 cells were pretreated with nanoparticles lacking FA (Gd₂O₃@PCD). In these cells, the T₁ signal intensity was approximately 2.3 times higher than in untreated controls, while the T₂ signal intensity decreased to 43% of the control value, as demonstrated by T₁- and T₂-weighted MRI data [21].

Since folic acid serves as a targeting ligand, in vitro MRI measurements confirmed a selective and increased intracellular uptake of Gd₂O₃@PCD–FA in M109 cancer cells compared to 4T1 cells [68]. A 2020 study found that at pH 5.5, the cumulative release of Lino-CUR was approximately 20% higher than at pH 7.4. In vitro MRI experiments demonstrated that Lino-CUR loaded onto FGO showed potential as a negative MRI contrast agent, effectively reducing signal intensity in MCF-10A and MCF-7 cells while exhibiting a sufficient relaxation rate (r₂ = 67.12 mM⁻¹s⁻¹). The strong negative contrast capability of FGO-Lino-CUR was further validated in in vivo MRI scans of tumor-bearing BALB/c mice [11].

Dual-mode agents offer greater diagnostic flexibility and reduce false positives. MnIO NPs with medium r_2/r_1 ratios (≈ 5 –7) successfully enabled both T_1 - and T_2 -weighted imaging [69]. In one study, $Gd_2O_3@PCD$ –FA NPs raised T_1 signal intensity 2.3-fold in folate-expressing tumors and reduced T_2 signal intensity by 50%. These balanced outcomes underscore the value of r_2/r_1 ratios between 4 and 7 for dual-mode contrast. Hybrid constructs (e.g., coreshell Fe₃O₄@Gd) achieve optimal contrast by spatially separating T_1 and T_2 materials. Clinical translation

depends on achieving reliable dual-contrast without interference between modalities.

Furthermore, this review identifies critical correlations between parameters. For example, particle size and surface charge jointly influence relaxivity and biodistribution, as smaller particles (<20 nm) with neutral or slightly negative coatings show better tumor penetration and longer circulation times. Similarly, polymer thickness correlates with both T₁ and T₂ relaxivity, as thicker coatings increase R₁ but may reduce R₂. The synergistic interaction between concentration and coating material also affects signal strength, where biocompatible coatings (e.g., PEG) at moderate concentrations (<0.5 mg/mL) optimize contrast while minimizing toxicity.

3.5. Combined Parameter Effects

Most studies assess nanoparticle parameters in isolation; however, recent work emphasizes the importance of integrated optimization. For instance, nanoparticles under 20 nm with PEGylated surfaces showed enhanced T₁ relaxivity and extended blood circulation when administered at concentrations below 0.5 mg/mL. Similarly, particles with dual coatings (e.g., PEG-silica) demonstrated balanced T₁/T₂ response and minimized immunogenicity. These synergistic effects highlight the necessity of coengineering size, surface charge, and coating thickness. An effective nanoparticle design must not only optimize magnetic relaxivity but also ensure long circulation times, tumor penetration, and low systemic toxicity. Future contrast agent development should adopt this multiparametric approach for superior diagnostic outcomes (Table 3).

The effectiveness of nanoparticle-based MRI contrast agents is not solely determined by individual parameters (size, concentration, coating) but rather by synergistic interactions. For instance, nanoparticles smaller than 20 nm with biocompatible PEG coatings demonstrate enhanced T₁ relaxivity and prolonged circulation time, while maintaining low cytotoxicity. This effect arises from the balance between high surface area for efficient water exchange (size), reduced protein adsorption (PEG coating), and optimal magnetic properties (concentration). Conversely, dual-layer coatings (e.g., PEG-silica) can achieve a balance between T₁ and T₂ relaxivity by

Parameter	Recommended Range	Effect on MRI Performance
Particle Size	5–20 nm	Enhances T ₁ relaxivity and tumor penetration
Concentration	0.1-0.5 mg/mL	Maximizes signal without quenching or cytotoxicity
PEG Coating Thickness	1–10 nm	Improves relaxivity and blood circulation
r ₂ /r ₁ Ratio (T ₁ agents)	< 5	Ensures bright T ₁ -weighted contrast
Shell Thickness (Silica)	< 10 nm	Prevents reduction in relaxivity from water shielding

Table 3. Threshold Ranges for Key Nanoparticle Parameters in MRI Optimization

modulating water proximity and magnetic response. These findings highlight that an integrated design approach—co-optimizing size, surface charge, coating, and concentration—is essential for developing efficient and safe MRI contrast agents [70].

3.6. Clinical Implications Summary

The findings of this systematic review offer several clinically relevant insights into the design of nanoparticle-based MRI contrast agents:

- Particle Size: Nanoparticles smaller than 20 nm consistently improve T₁ relaxivity and tumor penetration, making them ideal for highresolution imaging and early cancer detection.
- Concentration: Maintaining nanoparticle concentration within the range of 0.1–0.5 mg/mL ensures strong imaging signals while minimizing cytotoxic effects, balancing safety and diagnostic quality.
- Surface Coating: Hydrophilic and biocompatible coatings such as PEG, dextran, and silica not only enhance blood circulation and stability but also modulate magnetic response by improving relaxivity values.
- Dual-Mode Imaging: T₁-T₂ dual-mode nanoparticles with optimized r₂/r₁ ratios (between 4 and 7) can improve lesion characterization, reduce false positives, and enhance diagnostic reliability.
- Synergistic Design: The most promising contrast agents emerge from co-optimization of multiple parameters—particularly size, charge, and coating—rather than single-variable adjustments. Such integrated approaches are

essential for clinical translation and precision imaging.

These insights serve as a framework for developing next-generation contrast agents tailored for specific imaging goals, offering the potential to improve diagnostic accuracy and patient outcomes in clinical radiology.

3.7. Opportunities, Limitations, and Challenges

The integration of multiple materials nanoparticle-based MRI contrast agents presents both significant opportunities and notable challenges. Composites such as core-shell structures (e.g., Fe₃O₄(@Gd₂O₃) or hybrid systems incorporating iron oxide, gold, or silica allow simultaneous tuning of T1 and T2 relaxivity, offering dual-mode imaging capabilities [71]. For example, hybrid PEGylated MnFe₂O₄ nanoparticles encapsulated with silica and loaded with doxorubicin have shown enhanced r₁ and r₂ values alongside drug delivery potential, enabling theranostic applications [72]. Such combinations can also reduce toxicity by balancing magnetic performance with surface biocompatibility through selective coatings like HPG or dextran.

However, the synthesis of multifunctional agents introduces complexity in reproducibility, stability, and large-scale manufacturing. Disparate magnetic properties between T₁ and T₂ materials may interfere with one another, leading to contrast "cancellation" or inconsistent signal output. Moreover, thicker or multilayered coatings—while beneficial for stability—can increase hydrodynamic size, compromising tumor penetration and relaxivity. The variation in surface charge and binding affinities between materials also

affects biodistribution and clearance, complicating pharmacokinetics.

From a clinical standpoint, regulatory approval becomes more difficult when combining materials with separate safety profiles. Additionally, the lack of standardized relaxivity reporting across field strengths (e.g., 1.5T vs. 3T) further limits translational comparisons. Nonetheless, these limitations present opportunities for further innovation, particularly in designing smart, stimuli-responsive nanoparticles that adapt their magnetic and therapeutic behavior based on the tumor microenvironment.

Moving forward, the successful development of multi-material contrast agents will require interdisciplinary collaboration between materials scientists, radiologists, and pharmacologists to harmonize design, safety, and performance standards. Optimization strategies must focus on minimizing signal interference while maximizing contrast synergy, ensuring that complexity yields clinically meaningful advantages.

4. Conclusion

This systematic review highlights the critical role of nanoparticle size, surface coating, concentration, and functionalization in shaping the magnetic behavior and diagnostic performance of MRI contrast agents. Nanoparticles smaller than 20 nm demonstrated superior T₁ relaxivity, while concentrations within 0.1-0.5 mg/mL offered an optimal balance between Surface signal intensity and biocompatibility. modifications—particularly PEGylation, silica encapsulation, and dual-layer coatings-were shown to significantly enhance stability, relaxivity, and circulation time. Furthermore, combined parameter optimization, rather than single-variable focus, was essential in achieving effective and safe contrast enhancement, especially for dual-mode T₁/T₂ imaging.

A major strength of this review is its integration of quantitative relaxivity values and parameter thresholds from diverse studies, providing a clinically relevant synthesis rather than a purely descriptive summary. However, the review is limited by heterogeneity in study designs, MRI field strengths, and inconsistent reporting of in vivo versus in vitro results, which constrained the ability to conduct metaanalyses or standardized comparisons.

Future research should prioritize head-to-head comparisons of nanoparticle formulations under unified protocols, including standardized relaxivity reporting and long-term toxicity studies. Moreover, developing smart, stimuli-responsive, and multifunctional nanoplatforms tailored for specific clinical indications—such as early tumor detection or image-guided therapy—will be critical for translating laboratory innovation into clinical application.

Acknowledgement

This study was supported by the Medical Radiation Science Research Team, at Tabriz University of Medical Sciences, Tabriz, Iran.

This work was supported by the Tabriz University of Medical Sciences, Tabriz, Iran (Grant #70833) under the research ethics certificate ID: IR.TBZMED.VCR.REC.1401.384.

Due to the type of article, no human/animal use is applicable to this study. All the data associated with this systematic review is included in the article.

We would like to acknowledge the support provided by the Tabriz University of Medical Sciences, Tabriz, Iran, in conducting this research.

References

- 1- Jing Huang *et al.*, "Casein-Coated Iron Oxide Nanoparticles for High MRI Contrast Enhancement and Efficient Cell Targeting." *ACS applied materials & interfaces*, Vol. 504/30 (2013).
- 2- Guoming Huang *et al.*, "Tunable T-1 and T-2 contrast abilities of manganese-engineered iron oxide nanoparticles through size control." *Nanoscale*, Vol. 607/31 (2014).
- 3- Z. Y. Chen *et al.*, "Advance of molecular imaging technology and targeted imaging agent in imaging and therapy." (in eng), *Biomed Res Int*, Vol. 2014p. 819324, (2014).
- 4- Carlos Martínez-Boubeta *et al.*, "Learning from Nature to Improve the Heat Generation of Iron-Oxide Nanoparticles for Magnetic Hyperthermia Applications." *Scientific reports*, Vol. 3p. 1652, 04/11 (2013).
- 5- Azmi Aulia Rahmani, Qi Jia, Husein H. Bahti, Retna Putri Fauzia, and Santhy Wyantuti, "Recent advances in

- lanthanide-based nanoparticle contrast agents for magnetic resonance imaging: Synthesis, characterization, and applications." *OpenNano*, Vol. 21p. 100226, 2025/01/01/ (2025).
- 6- J. Wahsner, E. M. Gale, A. Rodríguez-Rodríguez, and P. Caravan, "Chemistry of MRI Contrast Agents: Current Challenges and New Frontiers." (in eng), *Chem Rev*, Vol. 119 (No. 2), pp. 957-1057, Jan 23 (2019).
- 7- D. Lau, P. G. Corrie, and F. A. Gallagher, "MRI techniques for immunotherapy monitoring." (in eng), *J Immunother Cancer*, Vol. 10 (No. 9), Sep (2022).
- 8- J. Bonlawar *et al.*, "Targeted Nanotheransotics: Integration of Preclinical MRI and CT in the Molecular Imaging and Therapy of Advanced Diseases." (in eng), *Nanotheranostics*, Vol. 8 (No. 3), pp. 401-26, (2024).
- 9- F. Garello *et al.*, "MRI detection of free-contrast agent nanoparticles." (in eng), *Magn Reson Med*, Vol. 93 (No. 2), pp. 761-74, Feb (2025).
- 10- C. Jacinto *et al.*, "Nanoparticles based image-guided thermal therapy and temperature feedback." (in eng), *J Mater Chem B*, Vol. 13 (No. 1), pp. 54-102, Dec 18 (2024).
- 11- N. Brown *et al.*, "Tuning ultrasmall theranostic nanoparticles for MRI contrast and radiation dose amplification." (in eng), *Theranostics*, Vol. 13 (No. 14), pp. 4711-29, (2023).
- 12- Seraj Mohaghegh, Tarighatnia Ali, Omidi Yadollah, Barar Jaleh, Aghanejad Ayuob, and Khosro and Adibkia, "Multifunctional magnetic nanoparticles for MRI-guided co-delivery of erlotinib and L-asparaginase to ovarian cancer." *Journal of Microencapsulation*, Vol. 39 (No. 4), pp. 394-408, 2022/05/19 (2022).
- 13- Fakhrosadat Sajjadian Ramin Ghasemi Shayan, "Sensitivity and Specificity Improvement for Breast Cancer Detection by Tumor-Microenvironment Multimodality Molecular Imaging." *Mathews J Case Rep.*, Vol. 8 (No. 10), p. 130, (2023).
- 14- Ramin Ghasemi Shayan, Tohid Mortezazadeh, and Mehdi Khalilnejad, "Article Acceptance Certificate Title: Application of Manganese Oxide (MnO) Nanoparticles in Multimodal Molecular Imaging and Cancer Therapy: A Review." *Nanomedicine*, Vol. 805/26 (2021).
- 15- Ramin Ghasemi Shayan, "Comprehensive Management of Prostate Cancer: From Diagnosis to Survivorship Postradiotherapy." *Oncology Advances*, (No. 000), (2024).
- 16- Tarighatnia Ali, Mahmoudi Golshan, Kiani Mahnaz, and Nader Nader, "Current Challenges and New Opportunities of Hybrid Nanoparticles for Diagnosis and Treatment of Cancer." *Frontiers in Biomedical Technologies*, Vol. 11 (No. 1), 01/01 (2024).
- 17- T. Tegafaw *et al.*, "Magnetic Nanoparticle-Based High-Performance Positive and Negative Magnetic Resonance Imaging Contrast Agents." (in eng), *Pharmaceutics*, Vol. 15 (No. 6), Jun 15 (2023).

- 18- J. Pellico, C. M. Ellis, and J. J. Davis, "Nanoparticle-Based Paramagnetic Contrast Agents for Magnetic Resonance Imaging." (in eng), *Contrast Media Mol Imaging*, Vol. 2019p. 1845637, (2019).
- 19- Ruth Antwi-Baah, Yajing Wang, Xiaoqin Chen, and Kui Yu, "Metal-Based Nanoparticle Magnetic Resonance Imaging Contrast Agents: Classifications, Issues, and Countermeasures toward their Clinical Translation." *Advanced Materials Interfaces*, Vol. 9 (No. 9), p. 2101710, (2022).
- 20- M. Habeeb, H. T. Vengateswaran, A. K. Tripathi, S. T. Kumbhar, H. W. You, and Hariyadi, "Enhancing biomedical imaging: the role of nanoparticle-based contrast agents." (in eng), *Biomed Microdevices*, Vol. 26 (No. 4), p. 42, Oct 23 (2024).
- 21- D. Zhang, J. Zhang, X. Bian, P. Zhang, W. Wu, and X. Zuo, "Iron Oxide Nanoparticle-Based T(1) Contrast Agents for Magnetic Resonance Imaging: A Review." (in eng), *Nanomaterials (Basel)*, Vol. 15 (No. 1), Dec 28 (2024).
- 22- W. Wang, X. Liu, X. Li, B. Geng, and E. Zhao, "Application of MRI imaging technology based on magnetic nanoparticles in diagnosis and prognosis evaluation of prostate cancer." (in eng), *SLAS Technol*, Vol. 29 (No. 6), p. 100225, Dec (2024).
- 23- A. Mali, E. L. Kaijzel, H. J. Lamb, and L. J. Cruz, "(19)F-nanoparticles: Platform for in vivo delivery of fluorinated biomaterials for (19)F-MRI." (in eng), *J Control Release*, Vol. 338pp. 870-89, Oct 10 (2021).
- 24- F. Mao and J. Zhou, "A needs analysis of ESP courses in colleges of art and design: Consensus and divergence." (in eng), *PLoS One*, Vol. 19 (No. 6), p. e0305210, (2024).
- 25- Zheyu Shen *et al.*, "Multifunctional Theranostic Nanoparticles Based on Exceedingly Small Magnetic Iron Oxide Nanoparticles for T1-Weighted Magnetic Resonance Imaging and Chemotherapy." *ACS Nano*, Vol. 11 (No. 11), pp. 10992-1004, (2017).
- 26- A. Amraee *et al.*, "Evaluation of ultra-small iron oxide nanoparticles as T1-weighted MRI contrast in cancerous tissues: a meta-analysis." *Clinical and Translational Imaging*, Vol. 10 (No. 4), pp. 403-11, 2022/08/01 (2022).
- 27- L. Zhu, H. Mao, and L. Yang, "Advanced iron oxide nanotheranostics for multimodal and precision treatment of pancreatic ductal adenocarcinoma." (in eng), *Wiley Interdiscip Rev Nanomed Nanobiotechnol*, Vol. 14 (No. 4), p. e1793, Jul (2022).
- 28- O. A. Kuchur, S. A. Tsymbal, M. V. Shestovskaya, N. S. Serov, M. S. Dukhinova, and A. A. Shtil, "Metalderived nanoparticles in tumor theranostics: Potential and limitations." (in eng), *J Inorg Biochem*, Vol. 209p. 111117, Aug (2020).
- 29- Z. Shi, P. Wang, L. Xie, and X. Zhao, "Biocompatible Au-Fe3O4 Nanoparticle-based Magnetic Resonance Imaging in the Diagnosis of Liver Tumor." (in eng), *Cell*

- Mol Biol (Noisy-le-grand), Vol. 68 (No. 3), pp. 59-66, Mar 31 (2022).
- 30- K. J. Chen *et al.*, "A small MRI contrast agent library of gadolinium(III)-encapsulated supramolecular nanoparticles for improved relaxivity and sensitivity." (in eng), *Biomaterials*, Vol. 32 (No. 8), pp. 2160-5, Mar (2011).
- 31- Y. Jiang *et al.*, "Relaxivity Enhancement of Hybrid Micelles via Modulation of Water Coordination Numbers for Magnetic Resonance Lymphography." (in eng), *Nano Lett*, Vol. 23 (No. 18), pp. 8505-14, Sep 27 (2023).
- 32- Y. You *et al.*, "Nanoparticle-enhanced synergistic HIFU ablation and transarterial chemoembolization for efficient cancer therapy." (in eng), *Nanoscale*, Vol. 8 (No. 7), pp. 4324-39, Feb 21 (2016).
- 33- Y. R. Zheng, Y. K. Chen, S. H. Lin, H. Cao, and Q. Chen, "Effect of High-Frequency Oscillatory Ventilation, Combined With Prone Positioning, in Infants With Acute Respiratory Distress Syndrome After Congenital Heart Surgery: A Prospective Randomized Controlled Trial." (in eng), *J Cardiothorac Vasc Anesth*, Vol. 36 (No. 10), pp. 3847-54, Oct (2022).
- 34- X. Mao, J. Xu, and H. Cui, "Functional nanoparticles for magnetic resonance imaging." (in eng), *Wiley Interdiscip Rev Nanomed Nanobiotechnol*, Vol. 8 (No. 6), pp. 814-41, Nov (2016).
- 35- M. Y. Ahmad *et al.*, "Functionalized Lanthanide Oxide Nanoparticles for Tumor Targeting, Medical Imaging, and Therapy." (in eng), *Pharmaceutics*, Vol. 13 (No. 11), Nov 8 (2021).
- 36- D. P. Seiter *et al.*, "Ferumoxytol dynamic contrast enhanced magnetic resonance imaging identifies altered placental cotyledon perfusion in rhesus macaques†." (in eng), *Biol Reprod*, Vol. 107 (No. 6), pp. 1517-27, Dec 10 (2022).
- 37- X. Dong *et al.*, "Magnetic resonance colonography with intestine-absorbable nanoparticle contrast agents in evaluation of colorectal inflammation." (in eng), *Eur Radiol*, Vol. 31 (No. 7), pp. 4615-24, Jul (2021).
- 38- S. Herz *et al.*, "Magnetic Particle Imaging Guided Real-Time Percutaneous Transluminal Angioplasty in a Phantom Model." (in eng), *Cardiovasc Intervent Radiol*, Vol. 41 (No. 7), pp. 1100-05, Jul (2018).
- 39- K. Szigeti *et al.*, "Thallium Labeled Citrate-Coated Prussian Blue Nanoparticles as Potential Imaging Agent." (in eng), *Contrast Media Mol Imaging*, Vol. 2018p. 2023604, (2018).
- 40- Leon Smith, Hilary L. Byrne, David Waddington, and Zdenka Kuncic, "Nanoparticles for MRI-guided radiation therapy: a review." *Cancer Nanotechnology*, Vol. 13 (No. 1), p. 38, 2022/11/12 (2022).
- 41- T. Mortezazadeh *et al.*, "Gadolinium (III) oxide nanoparticles coated with folic acid-functionalized poly(β -cyclodextrin-co-pentetic acid) as a biocompatible

- targeted nano-contrast agent for cancer diagnostic: in vitro and in vivo studies." (in eng), *Magma*, Vol. 32 (No. 4), pp. 487-500, Aug (2019).
- 42- K. Cheng, M. Yang, R. Zhang, C. Qin, X. Su, and Z. Cheng, "Hybrid nanotrimers for dual T1 and T2-weighted magnetic resonance imaging." (in eng), *ACS Nano*, Vol. 8 (No. 10), pp. 9884-96, Oct 28 (2014).
- 43- H. Seo *et al.*, "A DNA-Based MRI Contrast Agent for Quantitative pH Measurement." (in eng), *ACS Sens*, Vol. 6 (No. 3), pp. 727-32, Mar 26 (2021).
- 44- Amir Kazemi *et al.*, "Polydopamine-Coated Zn-MOF-74 Nanocarriers: Versatile Drug Delivery Systems with Enhanced Biocompatibility and Cancer Therapeutic Efficacy." *Journal of Inorganic and Organometallic Polymers and Materials*, Vol. 34 (No. 12), pp. 5718-31, 2024/12/01 (2024).
- 45- C. Sun, R. Sze, and M. Zhang, "Folic acid-PEG conjugated superparamagnetic nanoparticles for targeted cellular uptake and detection by MRI." (in eng), *J Biomed Mater Res A*, Vol. 78 (No. 3), pp. 550-7, Sep 1 (2006).
- 46- D. Patel, A. Kell, B. Simard, B. Xiang, H. Y. Lin, and G. Tian, "The cell labeling efficacy, cytotoxicity and relaxivity of copper-activated MRI/PET imaging contrast agents." (in eng), *Biomaterials*, Vol. 32 (No. 4), pp. 1167-76, Feb (2011).
- 47- C. Nwasike, E. Purr, E. Yoo, J. S. Nagi, and A. L. Doiron, "Activatable Nanoparticles: Recent Advances in Redox-Sensitive Magnetic Resonance Contrast Agent Candidates Capable of Detecting Inflammation." (in eng), *Pharmaceuticals (Basel)*, Vol. 14 (No. 1), Jan 16 (2021).
- 48- R. Bilardo, F. Traldi, A. Vdovchenko, and M. Resmini, "Influence of surface chemistry and morphology of nanoparticles on protein corona formation." (in eng), Wiley Interdiscip Rev Nanomed Nanobiotechnol, Vol. 14 (No. 4), p. e1788, Jul (2022).
- 49- Y. Nakamura, A. Mochida, P. L. Choyke, and H. Kobayashi, "Nanodrug Delivery: Is the Enhanced Permeability and Retention Effect Sufficient for Curing Cancer?" (in eng), *Bioconjug Chem*, Vol. 27 (No. 10), pp. 2225-38, Oct 19 (2016).
- 50- V. C. Deivayanai *et al.*, "A comprehensive review on advances in nanoparticle-mediated cancer therapeutics: Current research and future perspectives." *Cancer Pathogenesis and Therapy*, 2024/12/09/ (2024).
- 51- S. Surasinghe, I. Liatsou, Z. Nováková, C. Bařinka, D. Artemov, and S. Hapuarachchige, "Optical and MRI-Guided Theranostic Application of Ultrasmall Superparamagnetic Iron Oxide Nanodrug Conjugate for PSMA-Positive Prostate Cancer Therapy." (in eng), ACS Appl Mater Interfaces, Vol. 17 (No. 8), pp. 11611-23, Feb 26 (2025).
- 52- N. M. Ariyasingha *et al.*, "Developing Hyperpolarized Butane Gas for Ventilation Lung Imaging." (in eng),

- Chem Biomed Imaging, Vol. 2 (No. 10), pp. 698-710, Oct 28 (2024).
- 53- K. Y. Kim and K. A. Chang, "Therapeutic Potential of Magnetic Nanoparticle-Based Human Adipose-Derived Stem Cells in a Mouse Model of Parkinson's Disease." (in eng), *Int J Mol Sci*, Vol. 22 (No. 2), Jan 11 (2021).
- 54- J. S. Suk, Q. Xu, N. Kim, J. Hanes, and L. M. Ensign, "PEGylation as a strategy for improving nanoparticle-based drug and gene delivery." (in eng), *Adv Drug Deliv Rev*, Vol. 99 (No. Pt A), pp. 28-51, Apr 1 (2016).
- 55- N. Hoshyar, S. Gray, H. Han, and G. Bao, "The effect of nanoparticle size on in vivo pharmacokinetics and cellular interaction." (in eng), *Nanomedicine (Lond)*, Vol. 11 (No. 6), pp. 673-92, Mar (2016).
- 56- J. S. Ni, Y. Li, W. Yue, B. Liu, and K. Li, "Nanoparticle-based Cell Trackers for Biomedical Applications." (in eng), *Theranostics*, Vol. 10 (No. 4), pp. 1923-47, (2020).
- 57- T. R. Kyriakides *et al.*, "Biocompatibility of nanomaterials and their immunological properties." (in eng), *Biomed Mater*, Vol. 16 (No. 4), Mar 11 (2021).
- 58- Z. Amoozgar and Y. Yeo, "Recent advances in stealth coating of nanoparticle drug delivery systems." (in eng), *Wiley Interdiscip Rev Nanomed Nanobiotechnol*, Vol. 4 (No. 2), pp. 219-33, Mar-Apr (2012).
- 59- D. T. Savage, J. Z. Hilt, and T. D. Dziubla, "In Vitro Methods for Assessing Nanoparticle Toxicity." (in eng), *Methods Mol Biol*, Vol. 1894pp. 1-29, (2019).
- 60- M. Bellusci *et al.*, "Biodistribution and acute toxicity of a nanofluid containing manganese iron oxide nanoparticles produced by a mechanochemical process." (in eng), *Int J Nanomedicine*, Vol. 9pp. 1919-29, (2014).
- 61- E. Roy, S. Patra, R. Madhuri, and P. K. Sharma, "Stimuli-responsive poly(N-isopropyl acrylamide)-cotyrosine@gadolinium: Iron oxide nanoparticle-based nanotheranostic for cancer diagnosis and treatment." (in eng), *Colloids Surf B Biointerfaces*, Vol. 142pp. 248-58, Jun 1 (2016).
- 62- P. J. Hoopes *et al.*, "Imaging and modification of the tumor vascular barrier for improvement in magnetic nanoparticle uptake and hyperthermia treatment efficacy." (in eng), *Proc SPIE Int Soc Opt Eng*, Vol. 8584Feb 26 (2013).
- 63- G. Liang *et al.*, "Label-free, nucleotide-mediated dispersion of magnetic nanoparticles for "non-sandwich type" MRI-based quantification of enzyme." (in eng), *Biosens Bioelectron*, Vol. 41pp. 78-83, Mar 15 (2013).
- 64- Benedict You Wei Hsu *et al.*, "A Hybrid Silica Nanoreactor Framework for Encapsulation of Hollow Manganese Oxide Nanoparticles of Superior T1 Magnetic Resonance Relaxivity." *Advanced Functional Materials*, Vol. 25 (No. 33), pp. 5269-76, 2015/09/01 (2015).

- 65- Y. Sun *et al.*, "Metal-Organic Framework Nanocarriers for Drug Delivery in Biomedical Applications." (in eng), *Nanomicro Lett*, Vol. 12 (No. 1), p. 103, May 2 (2020).
- 66- R. Wei *et al.*, "Iron-oxide-based twin nanoplates with strong T(2) relaxation shortening for contrast-enhanced magnetic resonance imaging." (in eng), *Nanoscale*, Vol. 10 (No. 38), pp. 18398-406, Oct 4 (2018).
- 67- S. K. Golombek *et al.*, "Tumor targeting via EPR: Strategies to enhance patient responses." (in eng), *Adv Drug Deliv Rev*, Vol. 130pp. 17-38, May (2018).
- 68- S. Barua and S. Mitragotri, "Challenges associated with Penetration of Nanoparticles across Cell and Tissue Barriers: A Review of Current Status and Future Prospects." (in eng), *Nano Today*, Vol. 9 (No. 2), pp. 223-43, Apr 1 (2014).
- 69- T. Yang *et al.*, ""Targeting Design" of Nanoparticles in Tumor Therapy." (in eng), *Pharmaceutics*, Vol. 14 (No. 9), Sep 11 (2022).
- 70- H. Lee *et al.*, "Silica nanoparticle-based dual imaging colloidal hybrids: cancer cell imaging and biodistribution." (in eng), *Int J Nanomedicine*, Vol. 10 Spec Iss (No. Spec Iss), pp. 215-25, (2015).
- 71- Maryam Razaghi, Ali Ramazani, Mehdi Khoobi, Tohid Mortezazadeh, Eda Ayşe Aksoy, and Tuba Tüylü Küçükkılınç, "Highly fluorinated graphene oxide nanosheets for anticancer linoleic-curcumin conjugate delivery and T2-Weighted magnetic resonance imaging: In vitro and in vivo studies." *Journal of Drug Delivery Science and Technology*, Vol. 60p. 101967, 2020/12/01/(2020).
- 72- J. Fang *et al.*, "Manipulating the surface coating of ultrasmall Gd2O3 nanoparticles for improved T1-weighted MR imaging." (in eng), *Biomaterials*, Vol. 35 (No. 5), pp. 1636-42, Feb (2014).
- 73- Y. Li, W. Long, H. Zhou, T. Tan, and H. Xie, "Revolutionizing breast cancer Ki-67 diagnosis: ultrasound radiomics and fully connected neural networks (FCNN) combination method." (in eng), *Breast Cancer Res Treat*, Vol. 207 (No. 2), pp. 453-68, Sep (2024).
- 74- Tarighatnia Ali, Johal Gurkaran, Aghanejad Ayuob, Ghadiri Hossein, and Nader Nader, "Tips and Tricks in Molecular Imaging: A practical Approach." *Frontiers in Biomedical Technologies*, Vol. 8 (No. 3), 09/01 (2021).
- 75- Azadeh Amraee, Abolfazl Sarikhani, Leili Darvish, Zahra Alamzadeh, Rasoul Irajirad, and Seyed Rabie Mahdavi, "Curcumin Coated Ultra-Small Iron Oxide Nanoparticles as T1 Contrast Agents for Magnetic Resonance Imaging of Cancer Cells." *Journal of Biomedical Physics and Engineering*, Vol. 14 (No. 5), pp. 447-56, (2024).
- 76- Nasim Jamshidi, Ali Tarighatnia, Mona Ghaziyani, Fakhrossadat Sajadian, Maryam Olad-Ghaffari, and Nader Nader, Folic Acid-Conjugated Fe-Au-Based Nanoparticles for Dual Detection of Breast Cancer Cells

- by Magnetic Resonance Imaging and Computed Tomography. (2023).
- 77- M. A. Pysz, S. S. Gambhir, and J. K. Willmann, "Molecular imaging: current status and emerging strategies." *Clinical Radiology*, Vol. 65 (No. 7), pp. 500-16, 2010/07/01/ (2010).